Title

Pacific Warm Pool sub-surface heat sequestration modulated Walker Circulation and ENSO activity during the Holocene

One-sentence summaries

Orbital-driven Warm Pool upper-water heating regulates the equatorial Pacific climate change in the last 25000 years

Authors

Haowen Dang¹, Zhimin Jian^{1, *}, Yue Wang¹, Mahyar Mohtadi², Yair Rosenthal³, Liming Ye⁴, Franck Bassinot⁵, Wolfgang Kuhnt⁶

Affiliations

- ¹ State Key Laboratory of Marine Geology, Tongji University, Shanghai 200092, China.
- ² MARUM-Center for Marine Environmental Sciences, University of Bremen, 28359 Bremen, Germany.
- ³ Department of Marine and Coastal Science and Department of Earth and Planetary Sciences, Rutgers University, New Brunswick, NJ 08901, USA. 4 Key Laboratory of Submarine Geosciences, Second Institute of Oceanography, Ministry of Natural Resources of China, Hangzhou 310012, China.
- ⁵ Laboratoire des Sciences du Climat et de l'Environnement/IPSL, CEA-CNRS-UVSQ, University Paris-Saclay, 91198 Gif-sur-Yvette, France.
 - ⁶ Institute of Geosciences, Christian-Albrechts-University, D-24118 Kiel, Germany.
 - * Corresponding author. Email: jian@tongji.edu.cn

Abstract

The dynamics driving the El Niño Southern Oscillation (ENSO) over longer-than-interannual time-scales is poorly understood. A compilation of new and published records of thermal evolution in the Indo-Pacific Warm Pool thermocline over the past 25,000 years reveals a clear pattern characterized by a major warming in the Early Holocene and a secondary warming in the Middle Holocene. The first thermocline warming is likely related to the precession minimum and associated intensification of the southern Pacific shallow overturning circulation. The second thermocline warming is likely related to the September insolation maximum, which may have caused a steeper west-east thermal gradient in the equatorial Pacific upper-ocean and an intensified Walker Circulation. The Early- to Middle-Holocene thermocline warming in the Warm Pool is proposed to have ultimately reduced the inter-annual ENSO activity. Thus, a substantially increased oceanic heat content of the Warm Pool likely plays a role as a negative feedback for ENSO, particularly in the ongoing global warming.

Introduction

44

45

46

47

48

49

50 51

52

53

54

55

56

57

58

59

60

61

62

63

64 65

66

67

68

69

70

71

72

73

74

75

76 77

78

79

80

81

82

83

84

85

86

87

88

89

90

91

92

93

The equatorial eastern Indian and western Pacific Oceans with a persistent sea surface temperature (SST) above 28°C (termed the Indo-Pacific Warm Pool, IPWP) represent a major oceanic heat source for the atmosphere, characterized by deep atmospheric convection accompanied with heavy rainfall (1). The heat storage in the IPWP is essentially formed by the accumulation of warm surface waters driven by the equatorial trade winds (2) and modulated by the convergence of sub-surface ocean heat anomalies from North and South subtropical and eastern Pacific (3) (Fig. 1A). The west-east thermal asymmetry across the tropical Pacific and associated Walker Circulation play a key role in both the interannual variability of El Niño Southern Oscillation (ENSO) (2, 4) and the decadal to multidecadal Pacific climate changes (3, 4, 5). In association with the greenhouse warming over the 20th century, the equatorial Pacific west-east thermal gradient was possibly reduced, the Walker Circulation slowed down (6), and ENSO variability increased (4, 7). More recently, the slowdown of surface air warming between A.D. ~2000 and 2014 (aka "global warming hiatus") was featured by substantial cooling of equatorial Pacific SST, strengthening of the zonal thermal gradient and the Walker Circulation (3, 5), which has been attributed to enhanced heat storage in the equatorial Pacific thermocline (8, 9). It is not well understood, however, over decadal and even longer time-scales, how the upper ocean heat anomalies will vary with changes in the Walker Circulation, ENSO activity and the shallow overturning circulation from the sub-tropics, which can greatly improve our understanding and prediction of the future climate change.

On longer time-scales, from the last glacial maximum (LGM) to the Early Holocene, a warming of up to 4°C has been observed in the thermocline temperature records over the IPWP (10, 11, 12), possibly leading to a reduction of ENSO activity in the Early- to Middle-Holocene (13, 14). Additionally, stalagmite records from Borneo suggest that Walker Circulation was relatively weak during the last deglacial and strengthened in the Middle Holocene (15) when ENSO activity was suppressed (16). However, while the Borneo stalagmite record suggests similar-to-modern ENSO activity during the Early Holocene (16), other proxy records of ENSO activity from eastern equatorial Pacific indicate little or no ENSO activity during this period (17, 18). Such a discrepancy is largely caused by the sparsity of sediment core records and thus leads to an incomplete understanding of past changes in the upper ocean heat structure of the IPWP.

Here we present a compilation of over 30 sedimentary proxy-records (8 from this work) from the equatorial Pacific (Fig. 1A, Supplementary Table S1) to comprehensively examine changes in the upper-water (thermocline and above) temperature of the IPWP over the last ~25,000 years. We excluded five records (e.g., those from southwest Sumatra, 19) which are predominately influenced by local processes such as upwelling and do not reflect the general characteristics of IPWP's sub-surface (Supplementary Table S1). The records with an average temporal resolution of ~150 years constrained by a total of 217 radiocarbon dates (Methods, Table S2) covering the course of the LGM through the Holocene. The thermal structure of IPWP is examined by reconstructing temperatures of the thermocline water (TWT) and sea surface (SST) using shell Mg/Ca of two planktic foraminifera, the upperthermocline dweller *Pulleniatina obliquiloculata* (20, 21) and the mixed-layer dweller Globigerinoides ruber (21) (Methods). In order to minimize the possible inter-laboratory and inter-calibration biases and the effect of different cleaning protocols (Supplementary Information), we calculated the SST and TWT anomalies relative to the average value of each temperature record over 6-10 ka (denoted as SSTA and TWTA, Fig. 1B, D). The records of G. ruber δ^{18} O from 22 cores are processed in the same way to acquire the mean $\delta^{18}O_{G.\,ruber}$ anomaly ($\delta^{18}O_{G}$ -A, Fig. 1F), and are calculated for seawater $\delta^{18}O$ by subtracting the amount related to changes in local temperature and global ice-volume (22, Supplementary Information). Three deep thermocline temperature records of the eastern equatorial Pacific (EEP), estimated by shell Mg/Ca of *Neogloboquadrina dutertrei* are also analyzed (Supplementary Table S1).

Results

Mean TWTA and SSTA variations

The mean SSTA continuously warms by ~2.8±0.6°C since ~19 ka to ~10 ka, and cools by ~0.3±0.5°C from ~9 ka to 0 ka (ka: kilo annum, thousand years before AD1950, Fig. 1E), consistent with previous estimates (23, 24). The deglacial onset of positive SSTA occurs at ~18 ka with site-specific differences (25), which is generally synchronous with the onsets of the atmospheric pCO₂ rise (Fig. 1D), global mean sea-surface temperature warming (Fig. 1E), and decreases in the IPWP mean *G. ruber* δ^{18} O and the global benthic δ^{18} O stack (Fig. 1F).

The mean TWTA warms by $3.0\pm0.6^{\circ}\text{C}$ from ~22 ka to 11-9 ka and cools by $1.0\pm0.7^{\circ}\text{C}$ from 9 ka to 0 ka (Fig. 1B). The TWTA at 11-9 ka is highest and synchronous with the precession minimum and obliquity maximum (Fig. 1C). The onset of deglacial warming occurs at ~22 ka in TWTA, in-phase with the turning point of precession parameter (Fig. 1C) and precedes the deglacial pCO₂ rise (26) by ~4000 years (Fig. 1D). The deglacial mean TWTA warming mainly occurs in two phases: a first warming between 22 and 19 ka, coeval with the initial decrease of precession parameter, and a second warming between 13 and 11 ka, coinciding with the minima of precession parameter (Fig. 1B). The later warming phase is also synchronous with the final-phase in the deglacial rise of the atmospheric pCO₂ (Fig. 1D). The overall trend and the timing of the deglacial warming illustrate that orbital-driven insolation forcing controls the TWT change in the IPWP.

Besides the warm TWTA peak at ~11 ka, a second peak is found around 7-6 ka (Fig. 1B). In fact, TWT features observed in sites from open ocean differ from those within the Maritime Continent waters. The TWTA from open-ocean sites gradually warms from 22 ka and peaks at 11-10 ka (Fig. 2A), which we define as the Early-Holocene peak type (EHpeak). The near-equator TWTA records from the Maritime Continent waters are characterized by a rise after 15 ka and a Middle Holocene warm peak around 7 ka (Fig. 2B), defined as the Middle-Holocene peak type (MH-peak). The principal component analysis confirms the distinction, with a first principal component (Fig. 2C) yielding positive loadings for all records (Fig. 2D), and a second principal component (Fig. 2C) yielding different signs of loadings among the sites (Fig. 2E). The linear combinations of the first and second principal components resembles the two types of TWTA change (Fig. 2F), suggesting that "PC1-PC2" represents the feature of EH-peak type TWTA, and "PC1+PC2" the MH-peak type.

The Early-Holocene TWTA peak

The Early-Holocene peak type, consistent with the mean TWTA trend (Fig. 1B), is inphase with the changes in Earth's orbital configuration of precession and obliquity (Fig. 3A). The relationship between precession/obliquity and IPWP's thermocline change has been discovered before (10-12, 27, 28), and was explained by some regional oceanographic processes. Such a common Early-Holocene peak, however, implies a common driving mechanism over the entire IPWP thermocline. The western equatorial Pacific thermocline water originates from the basin-wide shallow overturning circulation of the Pacific Ocean

(1, 29), which is fed by the subduction of relatively salty, warm surface waters in the subtropical North and South Pacific (1), and is primarily regulated by the surface wind stress curls determined by the meridional SST gradients (30). Over the last 25 ka, the gradient between the southwestern Pacific SSTA (from 45.5°S,174.9°E) (31, 32) and the IPWP mean SSTA (Fig. 3B) resembles the Early-Holocene peak type TWTA, possibly reflecting relatively warmer mid-latitude and thereby enhanced warm water transport of shallow overturning circulation in the Early Holocene. In addition, for aminifer a δ^{13} C records of the equatorial Pacific also suggest an Early-Holocene intensification in the advection of southern-sourced sub-surface waters (33, 34). An Early-Holocene peak also appears in the southern Pacific and Antarctic temperature records due to the June (austral winter) insolation maximum at precession minimum (Supplementary Fig. S3). In modern observations (35), the northern Pacific shallow overturning circulation also contributes to the IPWP thermocline water, but the northwestern Pacific SSTA record shows no direct linkage to the Early-Holocene peak in IPWP thermocline (Supplementary Fig. S3). Therefore, we can only propose that the overall trend of IPWP's thermocline evolution over the LGM-Holocene may be dominated by the southern Pacific shallow overturning circulation, under the control of changing meridional insolation gradient induced by orbital forcing (i.e. precession and obliquity, 36).

Our hypothesized mechanism for the Pacific sub-surface temperature change is verified by a transient simulation of the Community Earth system model (CESM1.0.4, 37), forced by the orbital insolation and greenhouse gas changes of the past 300,000 years (38) (detailed in Methods). The responses of the Pacific upper-ocean thermal structure point out the key role played by precession in forming the Early-Holocene peak of TWT in the IPWP. At precession minimum during the Early Holocene, an intrusion of southern Pacific warm waters resulted in a drastic thermocline warming in the 30-200 m water depth of the openocean equatorial Pacific (140°E-140°W, Fig. 3C, D, E) and in the relatively deeper (below 120 m water depth) Maritime Continent waters (39) (100°E-140°E, Fig. 3F). Noteworthy, the precession minimum also induces significant cooling anomalies in the shallower Maritime Continent waters above 120 m depth in our simulation (Fig. 3F), in contrast to the paleo-proxy-based Early Holocene TWTA warming off the Philippines and in the Timor Sea. Therefore, the Early Holocene TWT warming in the IPWP may be a result of the precession-forced warming of deeper thermocline waters (Fig. 3D), which cannot be explained by the obliquity maximum with a cooling effect instead (Supplementary Fig. S4). Of course, the Early-Holocene warming may also be induced by the influence of increased atmosphere pCO₂, which results in a universal warming at all latitudes (Supplementary Fig. S4). In addition, the deglacial sea-level rise can also deepen the thermocline and result in thermocline warming in the Maritime Continent waters (40). Thus, the Early Holocene warming of the IPWP sub-surface water could have been caused by the combined effect of precession minimum, atmosphere pCO₂ maximum and sea-level high-stand.

The Middle-Holocene TWTA peak

144

145

146

147

148

149

150151

152

153

154

155

156

157

158

159

160

161162

163

164

165

166

167

168

169

170

171

172

173

174

175

176

177

178 179

180

181

182

183 184

185

186

187

188

189

190

191

192

193

For the near-equator sites within the Maritime Continent waters, the most significant thermocline warming occurs in the Middle Holocene. These records share two main features: (i) a cooling spell in 18-15 ka and (ii) a warming peak at ~7 ka (Fig. 4A). These sites are apparently less directly influenced by the southern Pacific sourced signal of the Early Holocene TWTA peak. The Middle Holocene peak type TWTA varies in-phase with the equatorial September insolation change (Fig. 4A) that dominates ENSO-related activities in the tropical Pacific (41). For example, the overall pattern of the MH-peak type TWTA is consistent with the W-E zonal temperature difference in both the sea surface (42)

and sub-surface across the equatorial Pacific, which show maxima in Middle Holocene and minima in the early stage of the deglaciation (Fig. 4B). Likewise, the strength of the ascending limb of the Walker Circulation, as indicated by the Borneo stalagmite $\delta^{18}O$ records, shows a minimum (more positive $\delta^{18}O$) around 17-16 ka and a maximum (more negative $\delta^{18}O$) around 7 ka (Fig. 4C), suggesting enhanced atmospheric convection over Borneo in the Middle Holocene.

The hydroclimate changes revealed by Borneo stalagmite are supported by our CESM simulation of annual mean rainfall timeseries over Borneo forced solely by orbital insolation change (Fig. 4C). In addition to the Borneo stalagmite records, the surface seawater $\delta^{18}O$ stack ($\delta^{18}O_{sw}$) of the IPWP shows positive excursions in the last deglacial and a negative peak in the Middle Holocene (Fig. 4D), indicating strengthened convective precipitation over evaporation in the Middle Holocene. Thus, we argue that the Middle Holocene thermocline warming of the near-equator IPWP is dynamically linked to the equatorial Pacific ENSO-like changes (e.g., enhanced Walker Circulation and strengthened W-E zonal thermal contrast in the Middle Holocene). Our model simulations verify that September insolation maximum forces a warming in the IPWP thermocline (Fig. 4E) and a stronger zonal thermal difference across the equatorial Pacific (Fig. 4F). The atmospheric response to an increased zonal thermal gradient leads to increased rainfall over western equatorial Pacific (Fig. 4G) and a stronger Walker Circulation (Fig. 4H).

Discussion

The long-term evolution of the tropical Pacific mean state, including the IPWP's thermocline temperature, the W-E temperature gradients and the western equatorial Pacific hydroclimate, have the potential to shape shorter-term climate oscillations, i.e. interannual ENSO activity, as suggested by simple model simulations (41, 43). In fact, an Early- to Middle-Holocene depression of ENSO activity associated with strengthening of the Walker Circulation relative to modern is evidenced by several proxy records and model simulations (13, 16, 44). Our findings suggest that, the evolution of the equatorial Pacific climate in response to precession forcing could be understood in analogy to the modern seasonal development of the equatorial Pacific air-sea coupled system (2). That is, in the Early Holocene under the precession minimum, the thermocline of the open-ocean IPWP warmed widely, thereby likely suppressing ENSO activity. During the Middle Holocene, maximal September insolation may have caused an overall thermocline warming, increased precipitation, and decreased sea surface salinity in the IPWP and strengthening of the Walker Circulation (Fig. 4D). A maximum in W-E upper-ocean thermal contrast (Fig. 4B) ultimately led to an extreme reduction of ENSO activity in the Middle Holocene.

The response of ENSO activity to future global warming and consequences to Earth's climate evolution are not well constrained by either modern observations or model simulations (45), thus necessitating additional observations from paleoclimate records. Our study shows that warming of the western equatorial Pacific thermocline coupled with increased W-E thermal gradient and strengthened Walker Circulation, may have ultimately led to the reduction in ENSO activity during the Early and Middle Holocene, when climate was arguably slightly warmer than at present (39, 46). This inference raises the possibility that enhanced anthropogenic heat sequestration in the western equatorial Pacific subsurface warm pool, through the shallow overturning cell and equatorial Pacific air-sea coupled system, may further augment heat uptake in the eastern equatorial Pacific cold tongue due to reduced ENSO activity. In the near future, these may subsequently lead to an intermittent

slowdown of surface warming, likely for short periods, in a pattern akin to the "global warming hiatus" between 2000 and 2014 (3, 5, 9).

Materials and Methods

We analyzed Mg/Ca and δ^{18} O of *G. ruber* (250-350 µm) and *P. obliquiloculata* (350-440 µm) at the State Key Laboratory of Marine Geology, Tongji University, Shanghai, PR China. Mg/Ca measurements were conducted on an ICP-MS (Thermo VG-X7) with measurement reproductivity of 2.2% for *G. ruber* (N=311) and 4.8% for *P. obliquiloculata* (N=302), estimated by replicate samples (N: total replicates of the 4 cores of this study, for details see Supplementary Table S2). Shell δ^{18} O of the two species was measured with a Finnigan-MAT253 mass spectrometer. Conversion to the international Pee Dee Belemnite (PDB) scale was performed using NBS19 standard, and the long-term variability of δ^{18} O is better than 0.07‰. Details of pre-treatments and procedures are described elsewhere (20).

The age models for the IPWP cores were all established mainly by linear relationships of radiocarbon dates, first corrected for the 14 C reservoir ages by the Marine Reservoir Correction and then calibrated to calendar age using CALIB7.1 software (http://calib.org) (Supplementary Tables S1 and S3). The time-series of proxies (SST, TWT and δ^{18} O) were then averaged at 150-yr non-overlapping bins using the stair-case integration re-sampling method. The temperature gradients of IPWP relative to the eastern equatorial Pacific or extra-tropical seas are calculated by the differences between the respective temperature anomaly records and on temporal steps determined by the average temporal resolution of the corresponding records (150 yr for W-E subsurface temperature gradient, 500 yr for W-E SST gradient, and 600 yr for South-Equatorial Pacific SST gradient).

Here we use the Community Earth System Model 1.0.4 (CESM) with T31 gx3v7 resolution (3.75°×3.75° for atmosphere and nominal 3° resolution for ocean, 37) to simulate the response of Pacific upper-ocean thermal structure to the forcing of orbital configuration (obliquity and precession) and change in atmospheric greenhouse gas content (GHG) (38). As a spin-up, the CESM was first run for 200 model years under orbital parameters and GHG of 300 ka and other boundary conditions in 1950 AD. Then the model was integrated for 3000 model years with the transient orbital insolation forcing and GHG changes of the past 300,000 years, in which orbital parameters and GHG were advanced by 100 years at the end of each model year (experiment CESM GHG). A similar transient accelerated experiment (CESM ORB) was only forced by orbital insolation changes since 300 ka (38). The outputs in the last 3000 model years of these two experiments were both analyzed, and they exhibit similar responses to orbital insolation forcing. Thus, only the results from experiment CESM GHG are shown. At first, ocean temperature, salinity, atmospheric circulation and precipitation are extracted from original outputs along multiple profiles (i.e. the latitude-longitude profile at 120 m water depth, the longitude-vertical profile along the equator, the latitude-vertical profile zonally averaged over the open Pacific (140°E-140°W) or the western Pacific (100°E-140°E)). Then these oceanic and atmospheric variables were linearly regressed onto the normalized timeseries of specific orbital forcing (i.e. obliquity parameter changes, GHG changes, and the June or September insolation changes defined by the solstice or equinox precessional mode, respectively, 38). Associated regression coefficients represent the Pacific air-sea coupled responses between maxima and minima of each orbital forcing. Statistical significance is assessed by the 95% confidence level of t test.

H2: Supplementary Materials

- Section S1: P. obliquiloculata Mg/Ca records and dissolution effect
- Section S2: Reconstructions of proxy data
- Fig. S1: P. obliquiloculata Mg/Ca records from different water depth
- Fig. S2: Comparison of the Mg/Ca-temperature records among calibrations and cleaning-methods
- Fig. S3: Comparison of the TWTA changes with other records
- Fig. S4: CESM simulated Pacific sub-surface temperature responses to obliquity and CO₂ forcings
- Table S1: The sediment cores analyzed in this study
- Table S2: Mg/Ca measurement reproductivity of core MD10-3340, SO18480, KX21-2 and MD01-2386
- Table S3: Radiocarbon dates of core MD10-3340, SO18480-3, KX973-21-2 and MD01-2386.

References and Notes

(References for the maintext: 1-49)

- 1. D. Gu, S. G. H. Philander, Interdecadal climate fluctuations that depend on exchanges between the tropics and extratropics. *Science* **275**, 805-807 (1997).
- 2. A. Timmermann, S.-I. An, J.-S. Kug, F.-F. Jin, W. Cai, A. Capotondi, K. M. Cobb, M. Lengaigne, M. J. McPhaden, M. F. Stuecker, El Niño—Southern Oscillation complexity. *Nature* **559**, 535-545 (2018).
- 3. S. McGregor, A. Timmermann, M. F. Stuecker, M. H. England, M. Merrifield, F.-F., Jin, Y. Chilkamoto, Recent Walker circulation strengthening and Pacific cooling amplified by Atlantic warming. *Nat. Clim. Change* **4**, doi: 10.1038/nclimate2330 (2014).
- 4. W. Cai, L. Wu, M. Langaigne, T. Li, S. McGregor, J.-S. Kug, J.-Y, Yu, M. F. Stuecker, A. Santoso, X. Li, Pantropical climate interactions. *Science* **363**, doi: 10.1126/science.aav4236 (2019).
- 5. M. H. England, S. McGregor, P. Spence, G. A. Meehl, A. Timmermann, W. Cai, A. S. Gupta, M. J. McPhaden A. Purich, A. Santoso, Recent intensification of wind-driven circulation in the Pacific and the ongoing warming hiatus. *Nat. Clim. Change* 4, doi: 10.1038/nclimate2106 (2014).
- 6. Z. Liu, Z. Jian, C. J. Poulsen, L. Zhao, Isotopic evidence for twentieth-century weakening of the Pacific Walker circulation. *Earth Planet. Sci. Lett.* **507**, 85-93 (2019).
- 7. W. Cai, G. Wang, B. Dewitte, L. Wu, A. Santoso, K. Takahashi, Y. Yang, A. Carr éric, M. J. McPhaden, Increased variability of eastern pacific El Niño under greenhouse warming. *Nature* **564**, 201-206 (2018).
- 8. N. Ramesh, R. Murtugudde, All flavours of El Niño have similar early subsurface origins. *Nat. Clim. Change* **3**, 42-46 (2013).
- 9. R. Neale, J. Slingo, The Maritime Continent and its role in the global climate: a GCM study. *J. Clim.* **16**, 834-847 (2003).
- 10. J. Xu, A. Holbourn, W. Kuhnt, Z. Jian, H. Kawamura, Changes in the thermocline structure of the Indonesian outflow during Terminations I and II. *Earth Planet. Sci. Lett.* **273**, 152-162 (2008).
- 11. T. Bolliet, A. Holbourn, W. Kuhnt, C. Laj, C. Kissel, L. Beaufort, M. Kienast, N. Andersen, D. Garbe-Schrönberg, Mindanao Dome variability over the last 160 kyr: Episodic glacial cooling of the West Pacific Warm Pool. *Paleoceanography* **26**, doi:10.1029/2010PA001966 (2011).
- 12. H. Dang, Z. Jian, F. Bassinot, P. Qiao, X. Cheng, Decoupled Holocene variability in surface and thermocline water temperatures of the Indo-Pacific Warm Pool. *Geophys. Res. Lett.* **39**, doi:10.1029/2011GL050154 (2012).
- 13. S. M. White, A. C. Ravelo, P.J. Polissar, Dampened El Niño in the Early and Mid-Holocene due to

insolation-forced warming/deepening of the thermocline. *Geophys. Res. Lett.* **45**, 316-326 (2018).

- 14. H. L. Ford, A. C. Ravelo, P. J. Polissar, Reduced El Niño-Southern Oscillation during the Last Glacial Maximum. *Science* **347**, 255-258 (2015).
 - 15. S. A. Carolin, K. M. Cobb, J. F. Adkins, B. Clark, J. L. Conroy, S. Lejau, J. Malang, A. A. Tuen, Varied response of western Pacific hydrology to climate forcings over the Last Glacial period. *Science* **340**, doi: 10.1126/science.1233797 (2013).
 - 16. S. Chen, S. S. Hoffman, D. C. Lund, K. M. Cobb, J. Emile-Geay, J. F. Adkins, A high-resolution speleothem record of western equatorial Pacific rainfall: implications for Holocene ENSO evolution. *Earth Planet. Sci. Lett.* **442**, 61-71 (2016).
 - 17. C. M. Moy, G. O. Seltzer, D. T. Rodbell, D. M. Anderson, Variability of El Nini/Southern Oscillation activity at millennial timescales during the Holocene epoch. *Nature* **420**, 162-165 (2002).
 - 18. J. L. Conroy, J. T. Overpeck, J. E. Cole, T. M. Shanahan, M. Steinitz-Kannan, Holocene changes in eastern tropical Pacific climate inferred from a Galapagos lake sediment record. *Quat. Sci. Rev.* 27, 1166-1180 (2008).
 - 19. X. Wang, Z. Jian, A. Lückge, Y. Wang, H. Dang, M. Mohtadi, Precession-paced thermocline water temperature changes in response to upwelling conditions off southern Sumatra over the past 300,000 years. *Quat. Sci. Rev.* **192**, 123-134 (2018).
 - 20. H. Dang, Z. Jian, J. Wu, F. Bassinot, T. Wang, C. Kissel, The calcification depth and Mg/Ca thermometry of *Pulleniatina obliquiloculata* in the tropical Indo-Pacific: A core-top study. *Mar. Micropaleontol.* **145**, 28-40 (2018).
 - 21. M. Hollstein, M. Mohtadi, Y. Rosenthal, P. M. Sanchez, D. Oppo, G. M. Méndez, S. Steinke, D. Hebbeln, Stable oxygen isotopes and Mg/Ca in planktic foraminifera from modern surface sediments of the Western Pacific Warm Pool: implications for thermocline reconstructions. *Paleoceanography* 32, doi: 10.1002/2017PA003122 (2017).
 - 22. C. Waelbroeck, L. Labeyrie, E. Michel, J.-C. Duplessy, J. F. McManus, K. Lambeck, E. Balbon, M. Labracherie, Sea-level and deep water temperature changes derived from benthic foraminifera isotopic records. *Quat. Sci. Rev.* **21**, 295-305 (2002).
 - 23. B. K. Linsley, Y. Rosenthal, D. W. Oppo, Holocene evolution of the Indonesian throughflow and the western Pacific warm pool. *Nat. Geosci.* **3**, 578-583 (2010).
 - 24. D. W. Lea, D. K. Pak, H. J. Spero, Climate impact of late Quaternary equatorial Pacific sea surface temperature variations. *Science* **289**, 1719-1724 (2000).
 - 25. J. F. Schröder, W. Kuhnt, A. Holbourn, S. Beil, P. Zhang, M. Hendrizan, J. Xu, Deglacial warming and hydroclimate variability in the central Indonesian Archipelago. *Paleoceanogr. Paleoclimatol.* **33**, doi: 10.1029/2018PA003323 (2018).
 - 26. S. A. Marcott, T. K. Bauska, C. Buizert, E. J. Steig, J. L. Rosen, K. M. Cuffey, T. J. Fudge, J. P. Severinghaus, J. Ahn, M. L. Kalk, Centennial-scale changes in the global carbon cycle during the last deglaciation. *Nature* **514**, doi:10.1038/nature13799 (2014).
 - 27. M. Hollstein, M. Mohtadi, Y. Rosenthal, M. Prange, D. W. Oppo, G. M. Méndez, K. Tachikawa, P. M. Sanchez, S. Steinke, D. Hebbeln, Variations in Western Pacific Warm Pool surface and thermocline conditions over the past 110,000 years: forcing mechanisms and implications for the glacial Walker Circulation. *Quat. Sci. Rev.* 201, 429-445 (2018).
 - 28. Z. Jian, Y. Wang, H. Dang, D. W. Lea, Z. Liu, H. Jin, Y. Yin, Half-precessional cycle of thermocline temperature in the western equatorial Pacific and its bihemispheric dynamics. *Proc. Natl. Acad. Sci. U.S.A.*, doi: 10.1073/pnas.1915510117 (2020).
 - 29. Z. Liu, M. Alexander, Atmospheric bridge, oceanic tunnel, and global climatic teleconnections. *Rev. Geophys.* **45**, doi: 10.1029/2005RG000172 (2007).
 - 30. Z. Liu, S.-I. Shin, B. Otto-Bliesner, J. E. Kutzbach, E. C. Brady, D. E. Lee, Tropical cooling at the last glacial maximum and extratropical ocean ventilation. *Geophys. Res. Lett.* **29**, doi: 10.1029/2001GL013938 (2002).
 - 31. K. Pahnke, J. P. Sachs, Sea surface temperatures of southern midlatitudes 0-160 kyr B. P. *Paleoceanography* **21**, doi:10.1029/2005PA001191 (2006).

32. K. Pahnke, R. Zahn, H. Elderfield, M. Schulz, 340,000-Year centennial-scale marine record of Southern Hemisphere climatic oscillation. *Science* **301**, doi: 10.1126/science.1084451 (2003).

- 33. J. Kalansky, Y. Rosenthal, T. Herbert, S. Bova, M. Altabet, Southern Ocean contributions to the Eastern Equatorial Pacific heat content during the Holocene. *Earth Planet. Sci. Lett.* **424**, 158-167 (2015).
- 34. S. C. Bova, T. Herbert, Y. Rosenthal, J. Kalansky, M. Altabet, C. Chazen, A. Mojarro, J. Zech, Links between eastern equatorial Pacific stratification and atmospheric CO₂ rise during the last deglaciation. *Paleoceanography* **30**, doi:10.1002/2015PA002816 (2015).
- 35. D. Hu, L. Wu, W. Cai, A. S. Gupta, B. Qiu, A. L. Gordon, X. Lin, Z. Chen, S. Hu, Pacific western boundary currents and their roles in climate. *Nature* **522**: doi:10.1038/nature14504 (2015).
- 36. S. G. Philander, A. V. Fedorov, Role of tropics in changing the response to Milankovich forcing some three million years ago. *Paleoceanography* **18**, 1045 (2003).
- 37. C. A. Shields, D. A. Bailey, G. Danabasoglu, M. Jochum, J. T. Kiehl, S. Levis, S. Park, The low-resolution CCSM4. *J. Clim.* **25**, 3993-4014 (2012).
- 38. Y. Wang, Z. Jian, P. Zhao, K. Xu, H. Dang, Z. Liu, D. Xiao, J. Chen, Precessional forced zonal triplepole anomalies in the tropical Pacific annual cycle. *J. Clim.* **32**(21), 7369-7402 (2019).
- 39. Y. Rosenthal, B. K. Linsley, D. Oppo, W. Pacific ocean heat content during the past 10,000 years. *Science* **342**, doi: 10.1126/science.1240837 (2013).
- 40. P. N. DiNezio, A. Timmermann, J. E. Tierney, F.-F. Jin, B. Otto-Bliesner, N. Rosenbloom, B. Mapes, R. Neale, R. F. Ivanovic, A. Montenegro, The climate response of the Indo-Pacific warm pool to glacial sea level. *Paleoceanography* **31**(6), 866-894 (2016).
- 41. A. C. Clement, R. Seager, M. A. Cane, Orbital control on the El Nino/Southern Oscillation and tropical climate. *Paleoceanography* **14**, 441-456 (1999).
- 42. A. Koutavas, S. Joanides, El Niño–Southern Oscillation extrema in the Holocene and Last Glacial Maximum. *Paleoceanography* **27**, doi:10.1029/2012PA002378 (2012).
- 43. R. Xie, F.-F. Jin, Two leading ENSO modes and El Niño types in the Zebiak-Cane model. *J. Clim.* **31**, 1943-1961 (2018).
- 44. M. Carré, J. P. Sachs, S. Purca, A. J. Schauer, P. Braconnot, R. A. Falcón, M. Julien, D. Lavallée, Holocene history of ENSO variance and asymmetry in the eastern tropical Pacific. *Science* **345**, doi: 10.1126/science.1252220 (2014).
- 45. A. V. Fedorov, S. G. Philander, Is El Nino Changing? Science 288, 1997-2002 (2000).
- 46. S. A. Marcott, J. D. Shakun, P. U. Clark, A. C. Mix, A reconstruction of regional and global temperature for the past 11,300 years. *Science* **339**, doi: 10.1126/science.1228026 (2013).
- 47. J. Laskar, P. Robutel, F. Joutel, M. Gastineau, A. C. M. Correia, B. Levrard, A long-term numerical solution for the insolation quantities of the Earth. *Astron. Astrophys.* **428**, 261-285 (2004).
- 48. J. D. Shakun, P. U. Clark, F. He, S. A. Marcott, A. C. Mix, Z. Liu, B. Ottoa-Bliesner, A. Schmittner, E. Bard, Global warming preceded by increasing carbon dioxide concentrations during the last deglaciation. *Nature* 484, doi:10.1038/nature10915 (2012).
- 49. L. E. Lisiecki, M. E. Raymo, A Pliocene-Pleistocene stack of 57 globally distributed benthic δ18O records. *Paleoceanography* **20**, doi:1010.1029/2004PA001071 (2005).
- 50. J. Yu, R. F. Anderson, Z. Jin, J. W. B. Rae, B. N. Opdyke, S. M. Eggins, Responses of the deep ocean carbonate system to carbon reorganization during the Last Glacial-interglacial cycle. *Quat. Sci. Rev.* **76**, 39-52 (2013).
- 51. W. Fan, Z. Jian, Z. Chu, H. Dang, Y. Wang, F. Bassinot, X. Han, Y. Bian, Variability of the Indonesian Throughflow in the Makassar Strait over the Last 30 ka. *Sci. Rep.* **8**, doi:10.1038/s41598-41018-24055-41591 (2018).
- 52. P. Anand, H. Elderfield, M. H. Conte, Calibration of Mg/Ca thermometry in planktonic foraminifera from a sediment trap time series. *Paleoceanography* **18**, doi:10.1029/2002PA000846 (2003).
- 53. Y. Rosenthal, S. Perron-Cashman, C. H. Lear, E. Bard, S. Barker, K. Billus, M. Bryan, M. L. Delaney, P. B. DeMenocal, G. S. Dwyer, Interlaboratory comparison study of Mg/Ca and Sr/Ca measurements in planktonic foraminifera for paleoceanographic research. *Geochem. Geophys. Geosyst.* 5,

doi:10.1029/2003GC000650 (2004).

- 54. P. A. Martin, D. W. Lea, A simple evaluation of cleaning procedures on fossil benthic foraminiferal Mg/Ca. *Geochem. Geophys. Geosyst.* **3**, doi:10.1029/2001GC000280 (2002).
 - 55. S. Barker, M. Greaves, H. Elderfield, A study of cleaning procedures used for foraminiferal Mg/Ca paleothermometry. *Geochem. Geophys. Geosyst.* **4**, doi:10.1029/2003GC000559 (2003).
 - 56. J. F. Schröder, A. Holbourn, W. Kuhnt, K. Küssner, Variations in sea surface hydrology in the southern Makassar Strait over the past 26 kyr. *Quat. Sci. Rev.* **154**, 143-156 (2016).
 - 57. A. Y. Sadekov, R. Ganeshram, L. Pichevin, R. Berdin, E. McClymont, H. Elderfield, A. W. Tudhope, Palaeoclimate reconstructions reveal a strong link between El Niño-Southern Oscillation and Tropical Pacific mean state. *Nat. Commun.* 4, doi: 10.1038/ncomms3692 (2013).
 - 58. L. D. Pena, I. Cacho, P. Ferretti, M. A. Hall, El Niño-Southern Oscillation-like variability during glacial terminations and interlatitudinal teleconnections. *Paleoceanography* **23**, doi: 10.1029/2008PA001620 (2008).
 - 59. M. Yamamoto, R. Suemune, T. Oba, Equatorward shift of the subarctic boundary in the northwestern Pacific during the last deglaciation. *Geophys. Res. Lett.* **32**, doi: 10.1029/2004GL021903 (2005).
 - 60. B. E. Bemis, H. J. Spero, J. Bijma, D.W. Lea, Reevaluation of the oxygen isotopic composition of planktonic foraminifera: experimental results and revised paleotemperature equations. *Paleoceanography* **13**, 150-160 (1998).
 - 61. J. Jouzel, V. Masson-Delmotte, O. Cattani, G. Dreyfus, S. Falourd, G. Hoffmann, B. Minster, J. Nouet, J.-M. Barnola, J. Chappellaz, Orbital and Millennial Antarctic Climate Variability over the Past 800,000 Years. *Science* 317, 793-796 (2007).
 - 62. E. J. Steig, E. J. Brook, J. W. C. White, C. M. Sucher, M. L. Bender, S. J. Lehman, D. L. Morse, E. D. Waddington, G. D. Clow, Synchronous climate changes in Antarctica and the North Atlantic. *Science* 282, 92-95 (1998).
 - 63. A. E. Shevenell, A. E. Ingalls, E. W. Domack, C. Kelly, Holocene Southern Ocean surface temperature variability west of the Antarctic Peninsula. *Nature* **470**, doi:10.1038/nature09751 (2011).
 - 64. Y. Wang, H. Cheng, R. L. Edward, J. Wu, C.-C. Shen, J. A. Dorale, A High-Resolution Absolute-Dated Late Pleistocene Monsoon Record from Hulu Cave, China. *Science* **294**, 2345-2348 (2001).
 - 65. C. A. Dykoski, R. L. Edwards, H. Cheng, D. Yuan, Y. Cai, M. Zhang, Y. Lin, J. Qing, Z. An, J. Revenaugh, A high-resolution, absolute-dated Holocene and deglacial Asian monsoon record from Dongge Cave, China. *Earth Planet. Sci. Lett.* **233**, 71-86 (2005).
 - 66. J. W. Partin, K. L. Cobb, J. F. Adkins, B. Clark, D. P. Fernandez, Millennial-scale trends in west Pacific warm pool hydrology since the Last Glacial Maximum. *Nature* **449**, 452-456 (2007).
 - 67. A. Timmermann, S. J. Lorenz, A.-I. An, A. Clement, S.-P. Xie, The effect of orbital forcing on the mean climate and variability of the tropical Pacific. *J. Clim.* **20**, doi: 10.1175/JCLI4240.1171 (2007).
 - 68. W. Fan, Z. Jian, F. Bassinot, Z. Chu, Holocene centennial-scale changes of the Indonesian and South China Sea throughflows: Evidences from the Makassar Strait. *Global Planet. Change* **111**, 111-117 (2013).
 - 69. H. Dang, Z. Jian, C. Kissel, F. Bassinot, Precessional changes in the western equatorial Pacific hydroclimate: A 240 kyr marine record from the Halmahera Sea, East Indonesia. *Geochem. Geophys. Geosyst.* **16**, 148-164 (2015).
 - 70. A. Holbourn, W. Kuhnt, J. Xu, Indonesian Throughflow variability during the last 140 ka: the Timor Sea outflow. *Geol. Soc. Spec. Publ.* **355**, 283-303 (2011).
 - 71. H. Dang, J. Wu, Z. Xiong, P. Qiao, T. Li, Z. Jian, Orbital and sea-level changes regulate the iron-associated sediment supplies from Papua New Guinea to the equatorial Pacific. *Quat. Sci. Rev.* **239**, doi: 10.1016/j.quascirev.2020.106361 (2020).
 - 72. Y. Rosenthal, D. W. Oppo, B. K. Linsley, The amplitude and phasing of climate change during the last deglaciation in the Sulu Sea, western equatorial Pacific. *Geophys. Res. Lett.* **30**, doi:10.1029/2002GL016612 (2003).
 - 73. L. Stott, A. Timmermann, R. Thunell, Southern Hemisphere and deep-sea warming led deglacial atmospheric CO₂ rise and tropical warming. *Science* **318**, doi: 10.1126/science.1143791 (2007).

- 74. K. Visser, R. Thunell, L. Stott, Magnitude and timing of temperature change in the Indo-Pacific warm pool during deglaciation. *Nature* **421**, 152-155 (2003).
- 75. C. Levi, L. Labeyrie, F. Bassinot, F. Guichard, E. Cortijo, C. Waelbroeck, N. Caillon, J. Duprat, T. de Garidel-Thoron, H. Elderfield, Low-latitude hydrological cycle and rapid climate changes during the last deglaciation. *Geochem. Geophys. Geosyst.* **8** doi:10.1029/2006GC001514 (2007).
- F. T. Gibbons, D. W. Oppo, M. Mohtadi, Y. Rosenthal, J. Cheng, Z. Liu, B. K. Linsley, Deglacial δ¹⁸O and hydrologic variability in the tropical Pacific and Indian Oceans. *Earth Planet. Sci. Lett.* 387, 240-251 (2014).
- 77. M. Hendrizan, W. Kuhnt, A. Holbourn, Variability of Indonesian Throughflow and Borneo runoff during the last 14 kyr. *Paleoceanography* **32**, 1054-1069 (2017).
- 78. R. Y. Setiawan, M. Mohtadi, J. Southon, J. Groeneveld, S. Steinke, D. Hebbeln, The consequences of opening the Sunda Strait on the hydrography of the eastern tropical Indian Ocean. *Paleoceanography* **30**, doi:10.1002/2015PA002802 (2015).
- 79. M. Mohtadi, A. Lückge, S. Steinke, J. Groeneveld, D. Hebbeln, N. Westphal, Late Pleistocene surface and thermocline conditions of the eastern tropical Indian Ocean. *Quat. Sci. Rev.* **29**, 887-896 (2010).
- 80. M. Mohtadi, M. Prange, D. W. Oppo, R. De Pol-Holz, U. Merkel, X. Zhang, S. Steinke, A. Lückge, North Atlantic forcing of tropical Indian Ocean climate. *Nature* **509**, doi:10.1038/nature13196 (2014).

Acknowledgments

General: We appreciate the sea-board assistance of cruises MD122, MD181, SO185 and KX08-973, and the laboratory assistance by Peijun Qiao, Weijia Fan and Zhihui Chu.

Funding: This study is supported by the National Natural Science Foundation of China (grants 91958208, 41976047, 41630965 and 91858106), the National Key Research and Development Program of China (grant 2018YFE0202401) and the Ministry of Natural Resources of China (grant GASI-GEOGE-04). MM acknowledges financial support by the BMBF grants 03G0806A (CARIMA) and 03G0864F (CAHOL). This study is implemented under the France-China Framework of LIA-MONOCL.

Author contributions: H.D. wrote the draft of the paper and all authors contributed to subsequent revisions; Z.J. designed the framework and H.D. proposed the preliminary idea of this research; Z.J. took lead in the experiments, assisted by H.D. and L.Y.; Y.W. carried out the numerical simulation; M.M. and Y.R. helped the interpretations; F.B. and W.K. provided part of the sediment materials and helped the AMS ¹⁴C measurements.

Competing interests: The authors declare that they have no competing interests.

Data and materials availability: The data that support the findings of this study are reported in the Supplementary Information. All the data can also be obtained from NOAA (ncdc.noaa.gov) and PANGAEA (pangaea.de), or from ZJ (email: jian@tongji.edu.cn).

Figures and Tables

Figure 1. Timeseries of thermocline and sea surface temperature anomalies in the IPWP compared to global climate indices during the past 25,000 years.

(A) Site locations of paired SST and TWT records (white circles) and SST-only records (blue triangles) (Supplementary Table S1). Shadings indicate temperatures at 120 m water depth. (B) Mean TWTA (red) of the IPWP records. Solid black arrows mark the two major warming phases of TWTA between 22-19 ka and 13-11 ka, respectively. (C) precession (dashed purple) and obliquity (orange) parameters (47). (D) Atmospheric pCO₂ derived from Antarctic WDC ice core (gray dots, 26). (E) Mean SSTA (blue) of the IPWP records and the global mean SST anomaly (Δ T, dark gray line, 48). (F) Mean IPWP *G. ruber* δ^{18} O_G anomaly (δ^{18} O_G-A, green) and LR04 benthic δ^{18} O stack (gray line and symbols, 49). Shadings of proxy records show the 1 σ standard deviation. Vertical dashed lines denote the timing of the deglacial onset of SST (~19 ka, blue) and TWT (~22 ka, red), the onset of the second deglacial warming step (gray) and the Early-Holocene peak of TWT (EH-peak, ~10.8 ka, red). Dotted red arrow denotes the Middle Holocene peak of TWT (MH-peak, 7 ka).

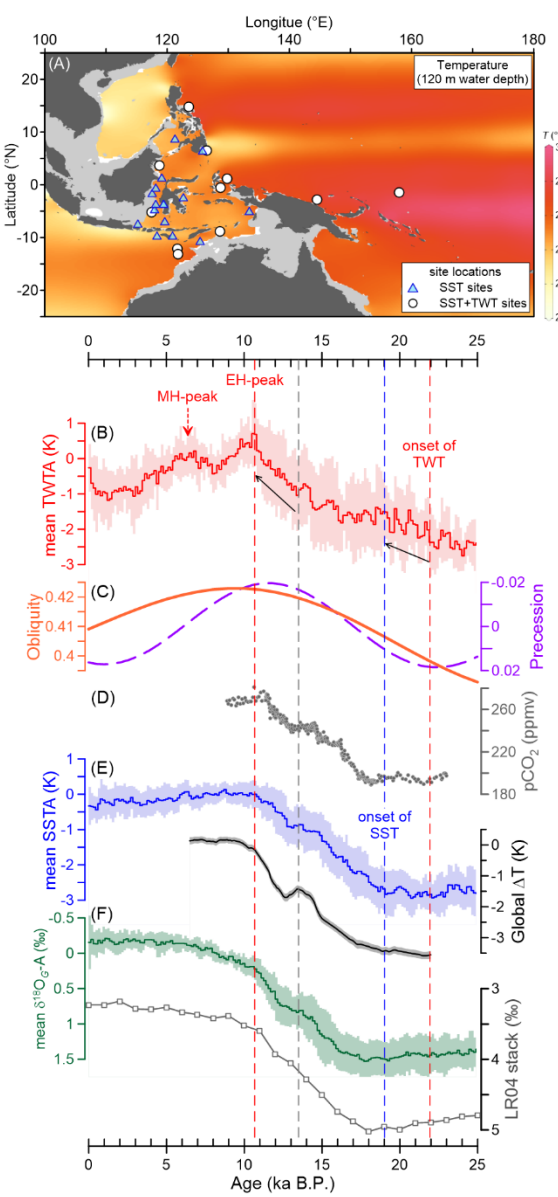


Figure 2. The two types of thermocline temperature anomaly (TWTA) records in the IPWP since the LGM.

(A) The average TWTA (brown) and the original TWTA records of the open-ocean sites. (B) Same as (A) but for the near-equator sites in the Maritime Continent waters. The TWT records in (A) and (B) are defined as Early-Holocene (EH) and Middle-Holocene (MH) peak types, respectively. (C) The first (blue) and second (red) principal components of all the TWTA records. PC1 and PC2 explain 62% and 16% of the total variance, respectively. (D, E) Loadings of PC1 (D) and PC2 (E) for each site. (F) Linear combinations of PC1 and PC2 that resemble the Early-Holocene peak type (PC1-PC2) and Middle-Holocene peak type (PC1+PC2), respectively.

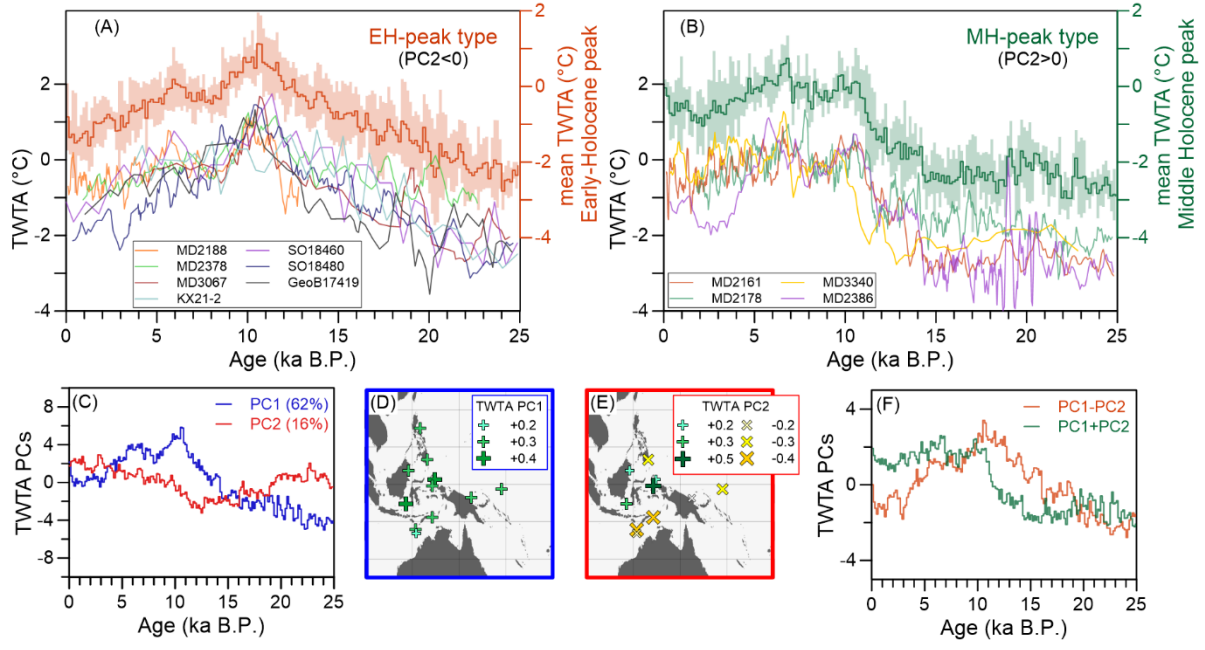


Figure 3. Precession-forced Early-Holocene TWTA peak.

(A) The mean TWTA of the Early-Holocene peak type (brown), precession (red dashed line) and obliquity (gray dotted line, 47). (B) Meridional SSTA gradient between southwest Pacific (SWP, site MD97-2120, from 45.5°S,174.9°E, 31-32) and the IPWP. Holocene, last Deglaciation, and LGM are separated by dashed vertical lines. CESM simulated responses of Pacific sub-surface temperature to June insolation in the Early Holocene are shown in (C-F): horizontal temperature anomaly distributions of upper-thermocline (at 120 m, C) and deeper thermocline (160-180 m water depths average, D), and meridional upper-water temperature anomaly profiles in the open Pacific (140°E-140°W, E) and the Maritime Continent waters (100°E-140°E, F). Temperature anomalies in (C-F) are shown as regression coefficients against the standardized time series of the June insolation at precessional band in experiment CESM_GHG. White shadings mask insignificant results below 95% confidence level (t-test).

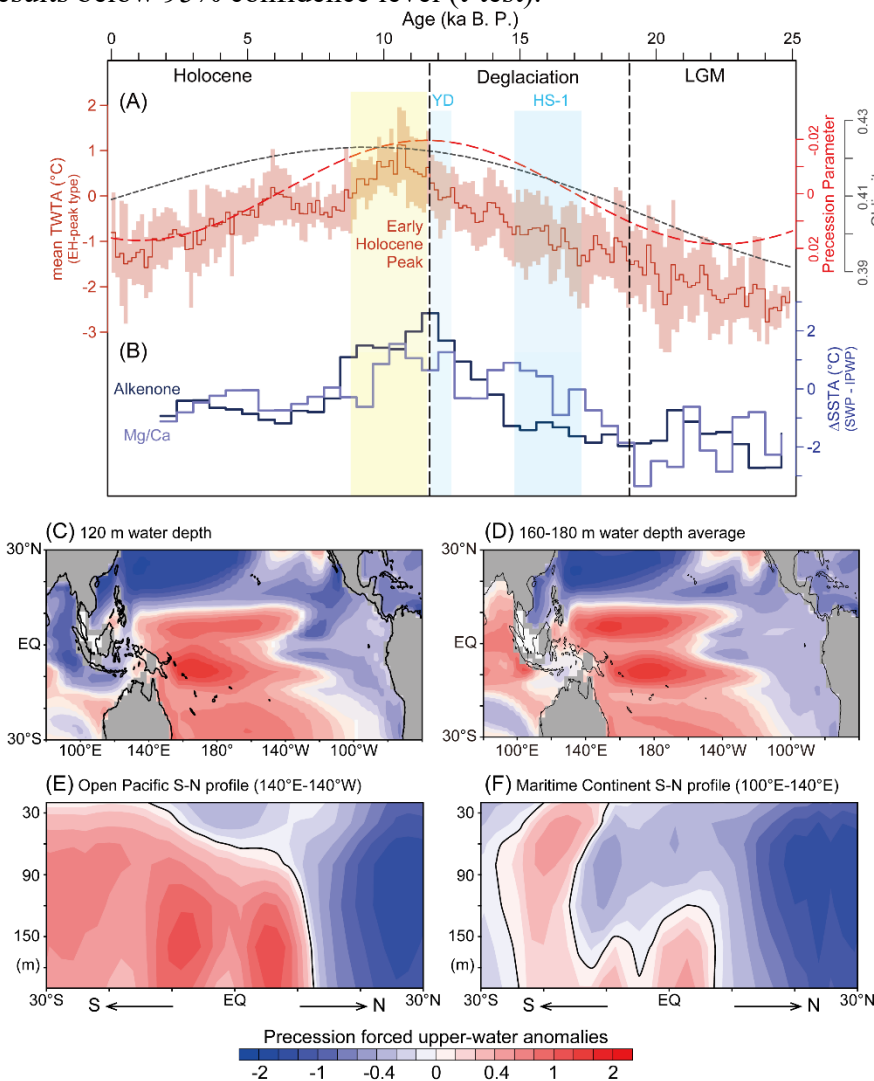


Figure 4. Timeseries and simulated temperature and rainfall anomalies in the IPWP since the LGM.

586587

588

589

590

591

592

593

594

595

596

597

598

599

600

601

602

603

604

605

606 607

(A) Mean TWTA of Middle-Holocene peak type (green) and the September 21st insolation at the Equator (dashed red line) and obliquity (gray dotted line, 47). (B) Zonal temperature gradients at sub-surface (Δ sub-TA, in gray) and at sea surface (Δ SSTA, light green, 42) shown as the difference between the WEP and EEP. (C) δ^{18} O records of northern Borneo stalagmites (15, 16) (dark and light green) and simulated annual mean rainfall (mm day⁻¹) over Borneo (dark gray, this study). (D) Mean anomaly of seawater δ^{18} O of IPWP (δ^{18} O_{sw}, dark gray, shading shows the standard deviation of the records). Shadings, vertical bars and dashed lines as in Fig. 3. Simulated response of the Pacific sub-surface temperature and atmospheric variables to September insolation maximum are shown in (E-H): (E) Annual mean TWTA at 120 m water depth. (F) Depth profile of the annual mean temperature anomaly across the Pacific between 5°S and 5°N. (G) Late autumn (October-to-December) anomalies of mean rainfall (colors, in mm day⁻¹) and horizontal winds at 850 hPa (arrows, in m s⁻¹, reference arrow on top right). (H) Late autumn mean Walker circulation anomalies between 5°S and 5°N across the Pacific, as indicated by anomalies in wind (arrows, in m s⁻¹, reference arrow on top right) and in vertical velocity (colors, in Pa s⁻¹). Positive values in red indicate upward motion and negative values in blue indicate downward motion. These anomalies in (E-H) are shown as regression coefficients against the standardized time series of the September insolation at precessional band in experiment CESM GHG.

